Sensors and Actuators B 199 (2014) 346–353

Contents lists available at ScienceDirect

Sensors and Actuators B: Chemical

journal homepage: www.elsevier.com/locate/snb

Hierarchical Fe_3O_4@Co_3O_4 core–shell microspheres: Preparation and acetone sensing properties

Fengdong Qu[a], Juan Liu[a], Ying Wang[a], Shanpeng Wen[b,*], Yu Chen[c,*], Xu Li[b], Shengping Ruan[a,*]

[a] State Key Laboratory on Integrated Optoelectronics, Changchun 130012, PR China
[b] College of Electronic Science and Engineering, Changchun 130012, PR China
[c] Institute of Semiconductors, Chinese Academy of Sciences, Beijing 100083, PR China

ARTICLE INFO

Article history:
Received 18 November 2013
Received in revised form 30 March 2014
Accepted 2 April 2014
Available online 13 April 2014

Keywords:
Fe_3O_4@Co_3O_4
Core–shell microspheres
Hydrothermal method
Gas sensor

ABSTRACT

Hierarchical Fe_3O_4@Co_3O_4 core–shell microspheres were prepared through a simple two-step hydrothermal method. The structure, morphology and surface characteristics of the microspheres were characterized by X-ray diffraction (XRD), X-ray photoelectron spectroscopy (XPS), scanning electron microscopy (SEM), energy dispersive X-ray spectroscopy (EDX), and Brunauer–Emmett–Teller (BET). The results showed that porous architectures were assembled from Fe_3O_4 sphere core and Co_3O_4 flower-like shells. The gas sensing investigations revealed that the Fe_3O_4@Co_3O_4 core–shell microspheres sensors exhibited enhanced sensing properties to acetone compared with Fe_3O_4 microspheres and Co_3O_4 nanomaterials, which might be attributed to the unique hierarchical structure and the synergetic effect exerted by Fe_3O_4 and Co_3O_4.

1. Introduction

Hierarchical oxide semiconductor core–shell nanostructure has demonstrated great potential applications in many fields, such as gas sensor [1–3], photocatalysis [4], lithium ion batteries [5], pseudocapacitive materials [6] and so on. Recently, many efforts have been devoted to the synthesis of hierarchical oxide semiconductor core–shell nanostructure by chemical vapor deposition [7], pulsed-laser deposition [8] and the epitaxial interfaces strategies [9], which are usually costly and complex. Besides, the above methods typically lack flexibility in structure. Solution phase route is considered to be an efficient method to synthesize core–shell nanostructure, which has the advantages of being economical, controllable in structure and environmental friendly. Lots of oxide semiconductor core–shell architectures have been assembled through a surfactant controlled growth in a hot organic solvent [10,11].

Being one of the bases of the functional materials, metal oxides semiconductor nanomaterials have great applications. Among them, Co_3O_4 is a vital p-type semiconductor with a normal spinel structure [12], and it has many commercial or potential application in solid-state sensors [13], anode materials in lithium ion batteries [14], heterogeneous catalysts [15]. Due to its high catalytic reactivity, Co_3O_4 is used as an oxidation agent for toxic gases and incompletely combusted gases. Thus, Co_3O_4 is expected to be a good candidate gas sensor. Typically, there are two ways to improve sensing performances, as has been reported. One is the use of nanostructured Co_3O_4 to modify or promote its intrinsic properties. The other is the use of cobalt oxide as an additive to achieve functional improvement to conventional gas sensors, due to its high effectivity as a receptor [16]. If it is made into a composite with an n-type semiconductor (such as ZnO), the sensitivity and selectivity can be enhanced. D. Bekermann et al. reported that Co_3O_4/ZnO nanocomposites exhibited an enhanced gas performance when comparing to bare Co_3O_4 [17]. Fe_3O_4 is a typical n-type semiconductor, and it is widely investigated as gas sensors [18,19], materials in lithium ion batteries [20] and so on. Although Co_3O_4 has made into composites with various n-type semiconductors, very little work has been directed toward fabricating gas sensors based on Co_3O_4/Fe_3O_4 composites, and there are few reports on the gas-sensing properties of Fe_3O_4@Co_3O_4 core–shell microspheres. Thus, synthesizing hierarchical Fe_3O_4@Co_3O_4 core–shell nanostructure has vitally scientific and practical significance.

In this work, we successfully synthesized hierarchical Fe_3O_4@Co_3O_4 core–shell microspheres by a two-step hydrothermal method. Firstly, Fe_3O_4 microspheres with diameter of about 0.6–1 μm were prepared. Subsequently, Fe_3O_4@Co_3O_4 core–shell nanostructure was assembled by a hydrothermal

* Corresponding authors. Tel.: +86 431 85168242; fax: +86 431 85168242.
E-mail addresses: sp_wen@jlu.edu.cn (S. Wen), chenyu_1099@163.com (Y. Chen), ruansp@jlu.edu.cn (S. Ruan).

http://dx.doi.org/10.1016/j.snb.2014.04.003
0925-4005/

process. Aiming to demonstrate the potential applications, the as-prepared materials were used to fabricate gas sensor. The results revealed that the Fe_3O_4@Co_3O_4 core–shell microspheres sensor exhibited a high response to acetone at optimum operating temperature of 160 °C, which was superior to bare Fe_3O_4 microspheres and bare Co_3O_4 nanomaterials.

2. Experimental

2.1. Chemical reagent

$FeSO_4·7H_2O$, urea, trisodium citrate, hydrochloric acid, butanol and ethanol were purchased from Beijing Chemicals Co., Ltd. (Beijing, China). $CoCl_2·6H_2O$ and $NaOAc·3H_2O$ were purchased from Xilong Chemical Reagent Co., Ltd. (Guangdong, China). All of these chemicals were analytical grade and used as received without further purification.

2.2. Synthesis process

2.2.1. Preparation of Fe_3O_4 microspheres and Co_3O_4 nanomaterials

$FeSO_4·7H_2O$ (0.4 mM, 0.11 g) was dissolved in ethanol (20 ml) to form a clear solution, followed by the addition of sodium acetate ($NaOAc·3H_2O$) (4 mM, 1.05 g) and trisodium citrate (Na_3Cit) (0.8 mM, 0.21 g). The mixture was stirred vigorously for 1 h and then transferred into a 30 ml Teflon-lined stainless-steel autoclave. The autoclave was heated to and maintained at 160 °C for 5 h, and then cool down to room temperature. The resulting black products were washed several times with deionized water and ethanol, and dried in vacuum at 60 °C for 4 h.

$CoCl_2·6H_2O$ (1 mM, 0.24 g) was dissolved in a 20 ml mixture of deionized water, ethanol and butanol (volume rate: 20:100:1). Then, the mixture was added trisodium citrate (Na_3Cit) (0.1 g) and urea (0.16 g). The mixture was stirred vigorously for 20 min and then transferred into a 30 ml Teflon-lined stainless-steel autoclave. The autoclave was heated to and maintained at 130 °C for 3 h, and then cool down to room temperature. The resulting red products were washed several times with deionized water and ethanol, and dried in vacuum at 60 °C for 4 h. Then the precursors were calcined at 300 °C for 1 h in air, and Co_3O_4 nanomaterials were obtained.

2.2.2. Synthesis of Fe_3O_4@Co_3O_4 core–shell nanostructures

The above obtained Fe_3O_4 microspheres were first treated in HCl (0.1 M) solution for 10 min under ultrasonic vibration. Then the microspheres were washed and transferred into a 30 ml Teflon-lined stainless-steel autoclave with a mixture of 11.6 ml deionized water, 8.3 ml ethanol and 0.1 ml butanol with $CoCl_2·6H_2O$ (1 mM, 0.24 g), Na_3Cit (0.1 g) and urea (0.16 g). The autoclave was heated to and maintained at 120 °C for 8 h, and then cool down to room temperature. The collected precursors were washed with deionized water and ethanol for many times and dried in a vacuum at 60 °C for 4 h. Then the precursors were calcined at 300 °C for 1 h in air, and the Fe_3O_4@Co_3O_4 core–shell nanostructures were obtained.

2.3. Characterization

X-ray diffraction (XRD) analysis was conducted on a Scintag XDS-2000 X-ray diffractometer with Cu Kα radiation (λ = 1.5418 Å). X-Ray photoelectron spectroscopy (XPS) data was obtained with a VG ESCALAB MK II spectrometer with an Mg KR excitation (1253.6 eV). Scanning electron microscopy (SEM) images were performed on a SHIMADZU SSX-550 (Japan) instrument. N_2 adsorption–desorption isotherms were measured at 77 K on a Micromeritics ASAP2000 system. Surface area and pore size distribution were evaluated using Brunauer–Emmett–Teller (BET) and Barrett–Joyner–Halenda (BJH) methods, respectively.

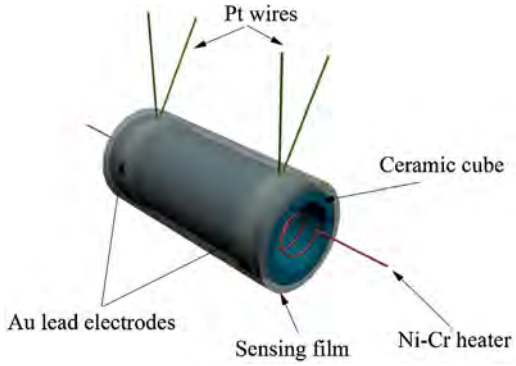

Fig. 1. Schematic structure of the gas sensor.

2.4. Fabrication and measurement of gas sensor

The as-prepared sample was mixed with deionized water in a weight ratio of 100:25 and ground in a mortar for 3 h to form a paste. The paste was then coated on a ceramic tube to form a sensing film (with a thickness of about 300 μm) on which a pair of Au electrodes was previously printed. Pt lead wires attaching to these electrodes were used as electrical contacts. After the ceramic tube was calcined at 300 °C for 2 h, a Ni-Cr heating wire was inserted in the tube as a heater for controlling the operating temperature. The structure of the sensor is shown in Fig. 1. The details of the sensor fabrication were similar to our previous works [21,22].

Gas sensing properties were measured by CGS-8 intelligent gas sensing analysis system (Beijing Elite Tech Co., Ltd., China) under room condition (25 °C,40 RH%). The test gases were injected into a test chamber by a microinjector. The response value (R) of p-type semiconductor (n-type semiconductor) was defined as $R = R_g/R_a$ ($R = R_a/R_g$), where R_g and R_a denoted the sensor's resistance in the absence and presence of the target gases (reducing gases). The time taken by the sensor to achieve 90% of the total resistance change was defined as the response time in the case of response (target gas adsorption) or the recovery time in the case of recovery (target gas desorption).

3. Results and discussion

3.1. Structural and morphological characteristics

The XRD pattern of the final product is shown in Fig. 2. It can be observed from Fig. 2(a) that the crystal phase of the final product was the mixture of Fe_3O_4 and Co_3O_4. Most of the diffraction peaks can be indexed to Co_3O_4, which was well agreed with the reported values from the Joint Committee on Powder Diffraction Standards card (JCPDS, 78-1970). The residual peaks were indexed to the magnetite structure of Fe_3O_4, which was consistent with the standard card file 75-0449. We can observe that the peaks of Fe_3O_4@Co_3O_4 cover those of Fe_3O_4 and Co_3O_4 from Fig. 2(b). Combined with EDX element analysis and XPS of the products, we can confirm the statement about presence of magnetite and absence of admixtures. EDX element mapping of the product were conducted. Fig. 3(a)–(d) showed element mapping of a single Fe_3O_4@Co_3O_4 core–shell microsphere. The distribution of Co was larger than that of Fe, which indicated the Fe_3O_4-core/Co_3O_4-shell structure. The EDX element analysis (Fig. 3(e)) revealed that the hierarchical core–shell microspheres consisted of Co, Fe and O elements. Besides, the Si element signal in the spectrum was attributed to the SEM grid used to support the sample. Besides, the XPS peaks of the

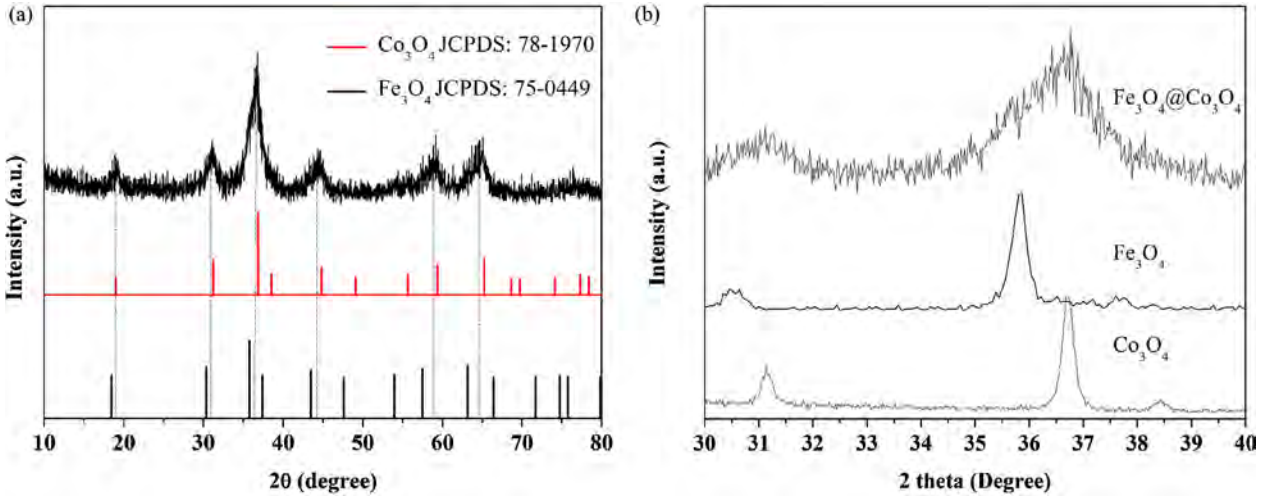

Fig. 2. (a) Full- and (b) part-XRD patterns of flowerlike Fe_3O_4@Co_3O_4 hierarchical microspheres obtained by calcining precursors at 300 °C for 1 h.

composite Fe_3O_4@Co_3O_4 core–shell nanostructures were indexed, which was shown in Fig. 4. As depicted in Fig. 4b, the peak centered at 781.1 eV corresponded to the Co $2p_{3/2}$ and another one centered at 796.4 eV was assigned to Co $2p_{1/2}$, and the energy difference between Co $2p_{3/2}$ and Co $2p_{1/2}$ splitting was 15.3 eV, which indicated the existence of both Co^{2+}/Co^{3+} [23,24]. Similarly, the peaks appearing in Fig. 4 (c) are located at 711.8 and 724.8 eV, which are ascribed to the Fe $2p_{3/2}$ and Fe $2p_{1/2}$ of Fe in Fe_3O_4 [25]. Thus, the obtained products are deduced to be Fe_3O_4 and Co_3O_4 composites.

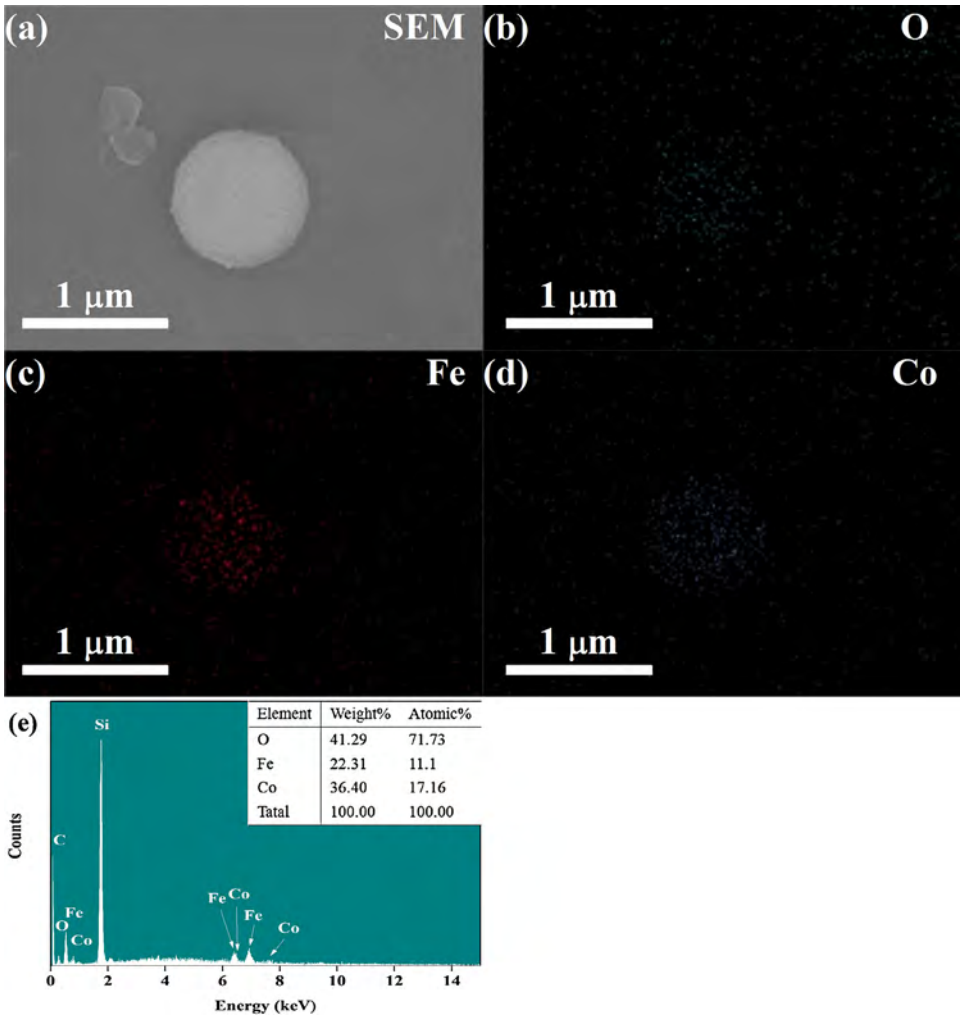

Fig. 3. (a) The SEM image of Fe_3O_4@Co_3O_4 hierarchical microsphere; (b–d) EDX elemental maps and (e) EDX spectra of the Fe_3O_4@Co_3O_4 hierarchical microspheres.

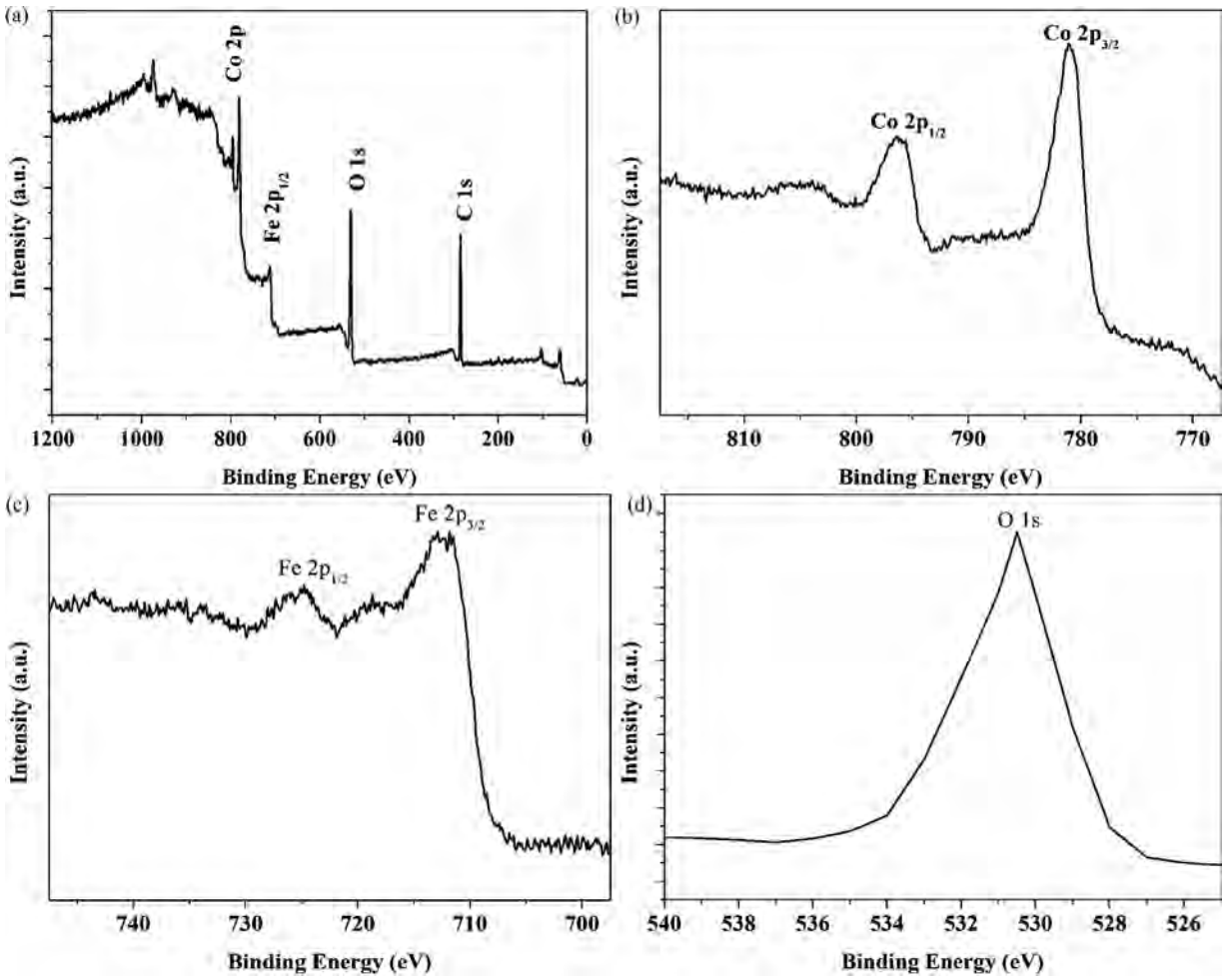

Fig. 4. XPS spectra of as-obtained flowerlike Fe_3O_4@Co_3O_4 hierarchical microspheres: (a) survey scan, (b) Co 2p spectrum, (c) Fe 2p spectrum and (d) O 1s spectrum.

The morphologies of the as-prepared hierarchical microspheres were investigated by SEM. Fig. 5(a) and (b) showed the low- and high-magnification SEM images of Fe_3O_4 microspheres, respectively. It could be observed from the images that the Fe_3O_4 microspheres had a relative uniform diameter of about 600–1000 nm. Fig. 5(c) and (d) showed the low- and high-magnification SEM images of Co_3O_4 nanomaterials, respectively. We can observe that the Co_3O_4 nanomaterials had flower-like surfaces which were similar to those of Fe_3O_4@Co_3O_4 core–shell microspheres. Fig. 5(e) showed a low-magnification SEM image of hierarchical Fe_3O_4@Co_3O_4 core–shell microspheres, and (f) showed a high-magnification SEM image of a single Fe_3O_4@Co_3O_4 core–shell microsphere with a small open hole, from which we can observe the core–shell structure. The sphere-like architectures had an average diameter of about 800 nm.

The surface structural characteristics of the as-prepared Fe_3O_4@Co_3O_4 core–shell structures were analyzed by nitrogen sorption isotherm techniques. As shown in Fig. 6(a), the isotherm profile should be categorized as type IV with a small hysteresis loop which indicates that mesoporous structure exists in microspheres [26]. The N_2-BET surface area of the Fe_3O_4@Co_3O_4 core–shell nanostructures was calculated to be 113.2 $m^2\,g^{-1}$, and the total pore volume was 0.530 $cm^3\,g^{-1}$. The pore-size distribution (Fig. 6(b)) was determined by using the BJH method from the desorption branch of the isotherm, the average pore diameter of the sample is about 5–30 nm (mesopores and macropores), which may be attributed to the Co_3O_4 flower-like shell (mesopores) and interparticular space (macropores).

3.2. Gas sensing properties

It is acknowledged that the gas response of a semiconductor sensor is usually dependent on the sensor operating temperature [27,28]. The responses of the sensor based on Fe_3O_4@Co_3O_4 core–shell nanostructure to 100 ppm acetone (C_3H_6O) and ethanol (C_2H_5OH) were tested to determine the optimum operating temperature, which were shown in Fig. 7(a). It can be observed that the responses of the tested sensor varied with operating temperature. According to Fig. 7(a), 160 and 140 °C were suggested to be the optimum operating temperature for acetone and ethanol detection, respectively, because the sensor showed the maximum response of 102.6 and 68.9 at the corresponding temperature. The variation in the optimum operating temperatures for acetone and ethanol could be understood by the dynamic equilibrium state of the initial adsorption and the subsequent desorption of the gases [29].

Fig. 8 showed the response transients of Fe_3O_4@Co_3O_4 core–shell nanostructure to various acetone concentration at 160 °C. It can be observed that the response shapes was approximately square, which indicated that the sensor responded rapidly and obtained an almost steady state [30]. When the sensor was exposed to air, the resistance returned nearly to the baseline level. The response times and the recovery times were shown in Table 1.

Fig. 9 presented the responses of Fe_3O_4@Co_3O_4 core–shell nanostructure, Co_3O_4 nanomaterials and Fe_3O_4 microspheres to different acetone concentrations at a working temperature of 160, 140 and 240 °C, respectively. The optimum operating temperature of Co_3O_4 nanomaterials and Fe_3O_4 microspheres were 140

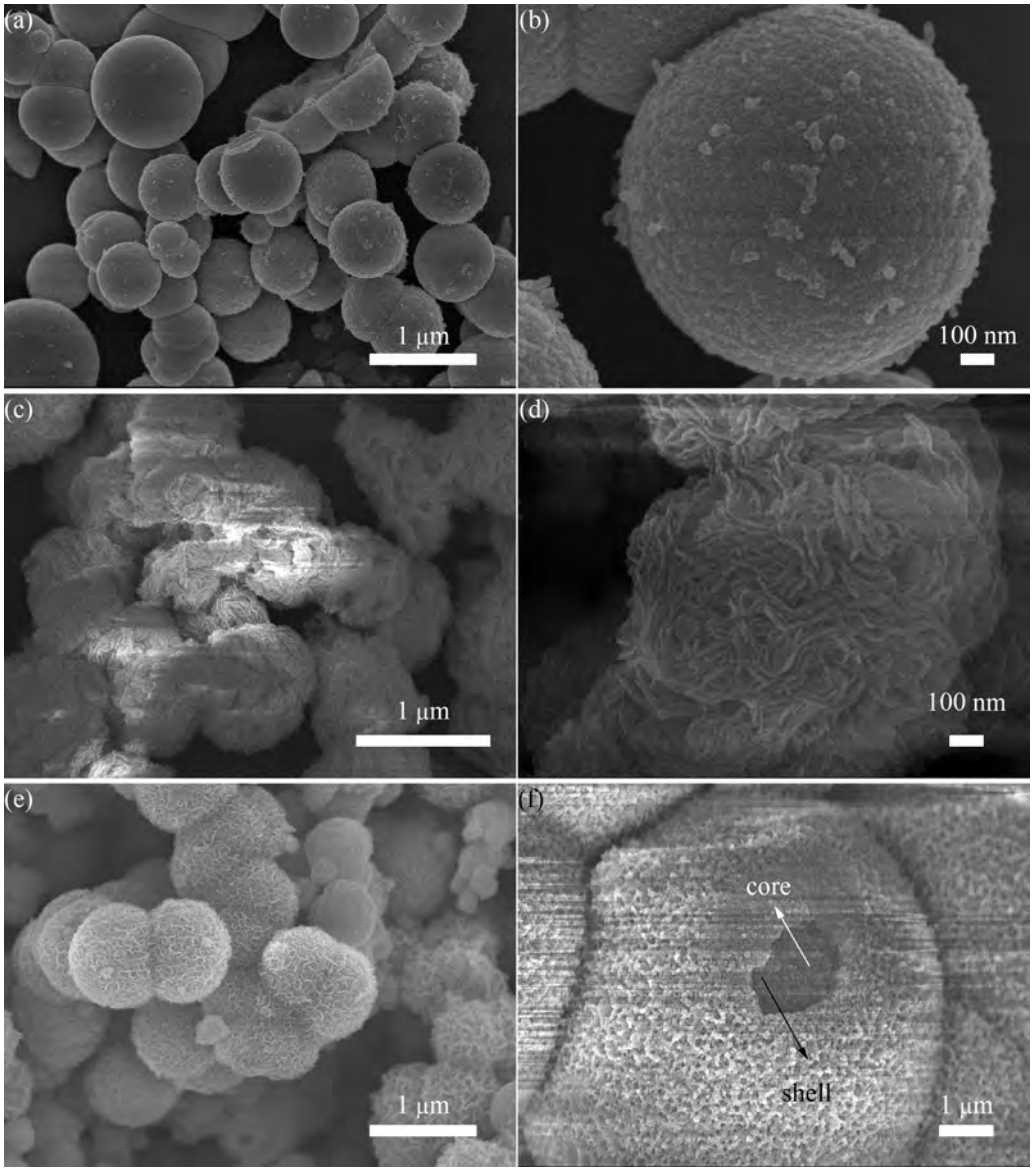

Fig. 5. Low (a) and high (b) magnification SEM images of the Fe_3O_4 microspheres; low (c) and high (d) magnification SEM images of the Co_3O_4 nanomaterials; low (e) magnification SEM image of Fe_3O_4@Co_3O_4 core–shell microspheres, and high (f) SEM image of a broken Fe_3O_4@Co_3O_4 core–shell microspheres.

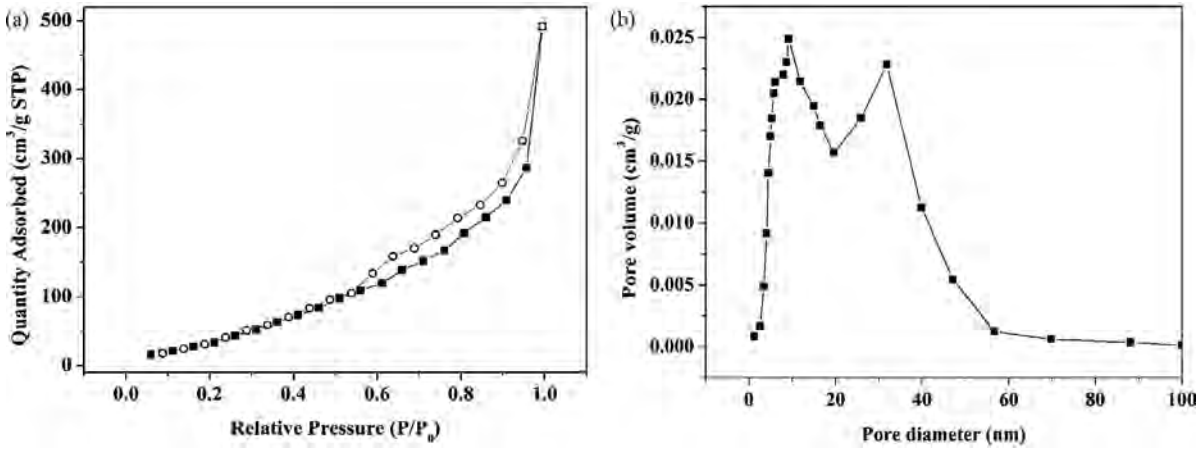

Fig. 6. (a) Typical N_2 adsorption–desorption isotherms and (b) pore-size distribution curve of Fe_3O_4@Co_3O_4 core–shell microspheres.

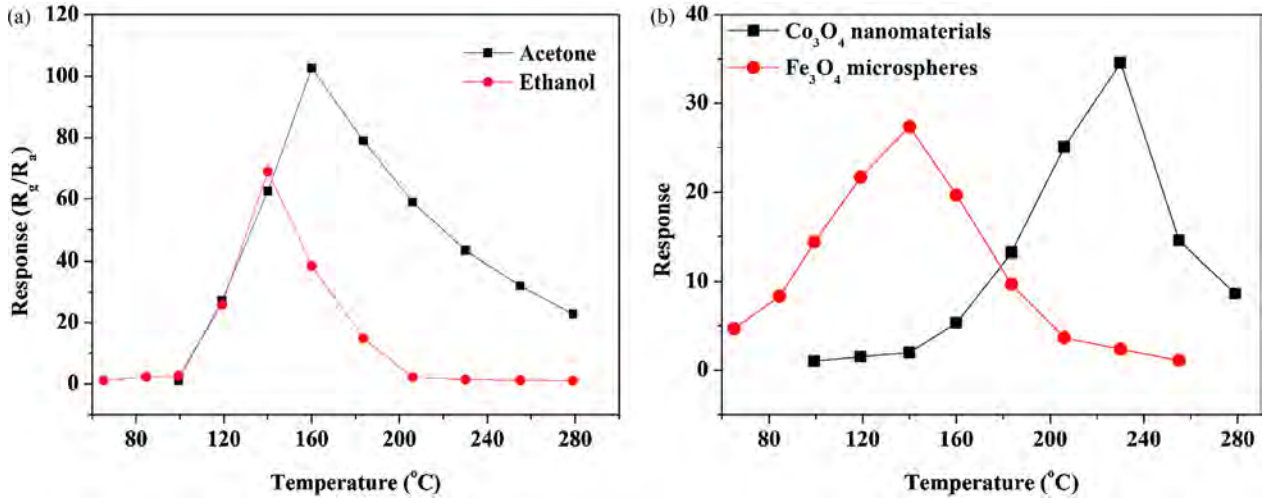

Fig. 7. Response of sensors based on (a) the as-prepared Fe_3O_4@Co_3O_4 core–shell microspheres to 100 ppm acetone, ethanol, (b) the as-prepared Fe_3O_4 microspheres and Co_3O_4 nanomaterials to 100 ppm acetone as a function of the operating temperature.

Table 1
Response and recovery time of the Fe_3O_4@Co_3O_4 core–shell microspheres sensor to various concentrations of acetone at 160 °C.

Concentration (ppm)	Response time (s)	Recovery time (s)
20	5	20
40	10	30
60	4	18
80	6	16
100	5	15

and 240 °C, respectively, which was shown in Fig. 7(b). With the increasing of the concentration of acetone, the responses of Fe_3O_4@Co_3O_4 core–shell nanostructure, Co_3O_4 nanomaterials and Fe_3O_4 microspheres all increased. It can be easily found that the responses increased rapidly with the increasing of acetone concentration (10–1000 ppm), and then gradually reached a response plateau (1000–5000 ppm). Besides, the Fe_3O_4@Co_3O_4 core–shell nanostructure sensor displayed enhancement in response to acetone compared to Fe_3O_4 microspheres (about 3–6 fold) and Co_3O_4 nanomaterials (about 2–4 fold). According to the inset of Fig. 9, the increase in the responses depended near linearly on the concentrations (from 10 to 100 ppm) for the Fe_3O_4@Co_3O_4 core–shell nanostructure sensor. The process may be involved adsorption as well as organic vapor reacting with O^- at surface. Under low acetone concentration (below 100 ppm), the rate of O_2 gas adsorption is relatively faster than that of acetone gas reacting with O^- at surface. With the acetone gas concentration increasing, the rate of acetone gas reacting with O^- is also increasing, for there are more acetone molecules that can participate in the reaction with the adsorbed O^-. Upon reaching the point of 100 ppm, the acetone gas molecules can be comparable with the reaction activation sites. With a further increasing of acetone concentration, the rate of acetone gas reacting with O^- increased slower compared with that under low acetone concentration. Thus, the response increased slowly when compared with that below 100 ppm. Finally, when the rate of acetone gas reacting with O^- reached a equilibrium with rate of oxygen re-adsorption on surface, the sensor comes into a saturation state.

A good selectivity is also a key parameter to a gas sensor. The selectivity of the sensor based on the as-prepared Fe_3O_4@Co_3O_4 core–shell nanostructure was measured on exposure to various gases at 200, 160, and 140 °C and the results were shown in Fig. 10. As can be seen in the figure, ethanol was less than 10% of acetone's response signal at the operating temperature of 200 °C, however, it was about 40% at 160 °C and 110% at 140 °C, respectively. Thus, the sensor had good selectivity to acetone over other gases at 200 °C.

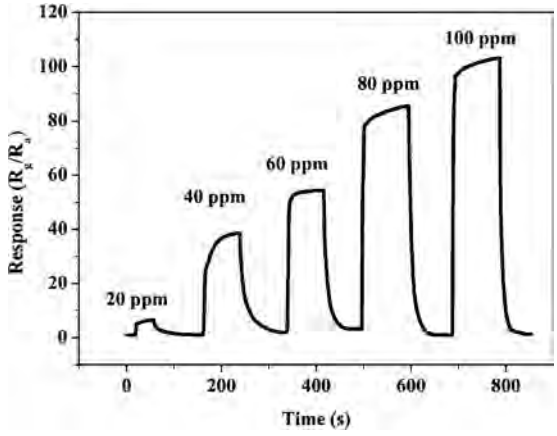

Fig. 8. Response transients of Fe_3O_4@Co_3O_4 core–shell microspheres to various acetone concentration at 160 °C.

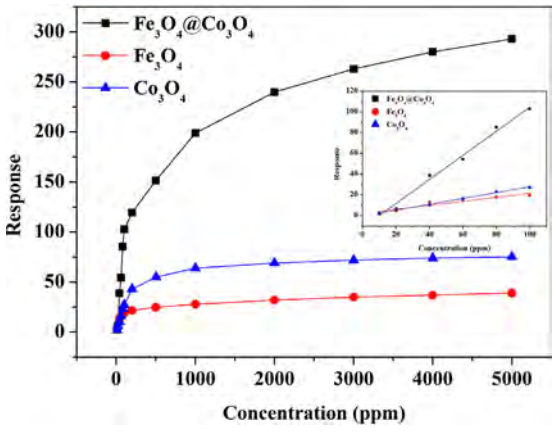

Fig. 9. Response of pure Fe_3O_4, Co_3O_4 and hierarchical Fe_3O_4@Co_3O_4 core–shell microspheres versus acetone concentrations.

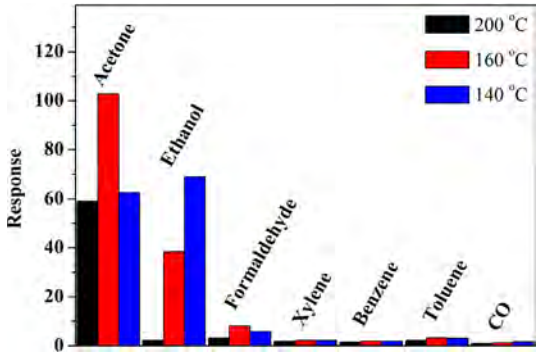

Fig. 10. Response of sensor based on hierarchical Fe_3O_4@Co_3O_4 core–shell microspheres to 100 ppm various gases at 200, 160, and 140 °C, respectively.

3.3. Gas sensing mechanism

In typically, Fe_3O_4 and Co_3O_4 are n-type and p-type semiconductor oxides, respectively, and their sensing mechanisms could be explained through the change in resistance of the sensor caused by the adsorption and desorption process of oxygen molecules on the surface of the oxides [13,19,31]. When a p-type oxide semiconductor sensor is exposed to air, the oxygen in the air (carrier gas) captures the electrons from the sensing materials and ion-adsorbed O_2^-, O^- and O^{2-} on the surface of sensing layer, resulting in an increase of the carrier density and the formation of a conduction layer on the surface of the sensing materials. On exposure to acetone and ethanol (reducing gases), the gases molecules will react with pre-adsorbed oxygen (Eqs. (1) and (2)). The reaction releases free electrons, which neutralize the holes in the p-type oxide semiconductor (Eq. (3)), thereby increasing the measured resistance [32]. The solution of the n-type oxide semiconductor sensor is the inverse condition [33]

$$C_3H_6O(ads) + 8O^-(ads) \leftrightarrow 3CO_2(gas) + 3H_2O(gas) + 8e^- \quad (1)$$

$$C_2H_5OH(ads) + 6O^-(ads) \leftrightarrow 2CO_2(gas) + 3H_2O(gas) + 6e^- \quad (2)$$

$$e^- + h^\bullet \leftrightarrow Null \quad (3)$$

The gas sensing property of the as-synthesized Fe_3O_4@Co_3O_4 core–shell nanostructure sensor for acetone was much better than that of Fe_3O_4 microspheres and Co_3O_4 nanomaterials. The enhanced sensing properties are likely to be related to the following factors. Firstly, the synergetic effect of different gas sensing materials is considered for both Fe_3O_4 and Co_3O_4 are important sensing materials. The effect has been observed in other hierarchical core–shell nanostructures [3,34]. Consequently, the synergetic effect of two different gas sensing materials in composites requires two factors. The first one is that the thickness of the shell materials is close to its Debye length (λ_D). Besides, the core and the shell materials should have strong response to the target gas [a]. The value of λ_D can be calculated by the following equation,

$$\lambda_D = \left(\frac{\varepsilon\kappa T}{q^2 n_C}\right)^{1/2}, \quad (4)$$

where ε is the static dielectric constant, κ is the Boltzmann's constant, T is an absolute temperature (K), q is the electrical charge of the carrier, and n_C is the carrier concentration [b]. For bulk Co_3O_4, assuming n_C is $5 \times 1018\,cm^{-3}$, λ_D is about 40 nm at the operating temperature of 160 °C according to Eq. (4). In our work, the thickness of the Co_3O_4 shell was estimated to be about 50 nm, which could be comparable with its λ_D. As to the second factor, both the Fe_3O_4 microspheres core and Co_3O_4 nanomaterials shell have relativity large response to acetone. Besides, the sensor based on Fe_3O_4@Co_3O_4 flower-like microspheres exhibited enhanced gas response to acetone compared with the sensor based on Fe_3O_4 microspheres core and Co_3O_4 nanomaterials. Besides, the well-known catalytic activity of cobalt oxide is believed to play a further beneficial role on the functional behavior. It means that n-type metal oxides only chemisorb as much oxygen as possible to compensate their deficiencies [35]. However, the concentration of surface oxygen on p-type materials is significantly higher [36,37]. As a result, the co-presence of Co_3O_4 and Fe_3O_4, having an intimate contact between them, can further contribute to the improvement of the composite sensor performances. Judging from the evidence above, we believe this so-called "synergetic effect" does exist.

Second, it is the unique hierarchical structure that may attribute to enhance the gas sensing properties. The p-Co_3O_4/n-Fe_3O_4 junction, which was shown in Fig. 5(f), produce an improved charge separation at the interface between the two oxides, generating, in turn, an enhanced conductance modulation on interaction with target gases. Consequently, the Fe_3O_4@Co_3O_4 core–shell nanostructure exhibits an enhanced sensing property [17]. A further detailed sensing mechanism of Fe_3O_4@Co_3O_4 core–shell microspheres is still under investigation by our group.

4. Conclusions

In conclusion, we reported the synthesis of Fe_3O_4@Co_3O_4 core–shell microspheres through hydrothermal method and investigated the acetone sensing properties. An enhanced sensing property to acetone was observed, which was superior to bare Fe_3O_4 microspheres and Co_3O_4 nanomaterials. The enhanced gas sensing properties were probably attributed to the synergetic effect of Fe_3O_4 and Co_3O_4 as well as the assembled heterojunction. The results demonstrate that the hierarchical core–shell microspheres sensor is a potential candidate for high performance gas sensors.

Acknowledgments

This work was supported by the National Natural Science Foundation of China (Grant Nos. 61274068, and 61275035), Chinese National Programs for High Technology Research and Development (Grant No. 2013AA030902), Project of Science and Technology Development Plan of Jilin Province (Grant Nos. 20120324 and 20130206021GX), and the Opened Fund of the State Key Laboratory on Integrated Optoelectronics (No. IOSKL2012KF03).

References

[1] P. Sun, Y. Sun, J. Ma, L. You, G. Lu, W. Fu, et al., Synthesis of novel SnO_2/$ZnSnO_3$ core–shell microspheres and their gas sensing properities, Sens. Actuators B 155 (2011) 606–611.
[2] W. Guo, T. Liu, R. Sun, Y. Chen, W. Zeng, Z. Wang, Synthesis of unique ZnO/SnO_2 core–shell structural microspheres and their gas-sensing properties, Mater. Lett. 89 (2012) 5–8.
[3] Y.-J. Chen, G. Xiao, T.-S. Wang, F. Zhang, Y. Ma, P. Gao, et al., α-MoO_3/TiO_2 core/shell nanorods: controlled-synthesis and low-temperature gas sensing properties, Sens. Actuators B 155 (2011) 270–277.
[4] M. Ye, Q. Zhang, Y. Hu, J. Ge, Z. Lu, L. He, et al., Magnetically recoverable core–shell nanocomposites with enhanced photocatalytic activity, Chemistry – A European Journal 16 (2010) 6243–6250.
[5] J. Liu, W. Li, A. Manthiram, Dense core–shell structured SnO_2/C composites as high performance anodes for lithium ion batteries, Chem. Commun. 46 (2010) 1437–1439.
[6] J. Liu, J. Jiang, C. Cheng, H. Li, J. Zhang, H. Gong, et al., Co_3O_4 nanowire@MnO_2 ultrathin nanosheet core/shell arrays: a new class of high-performance pseudocapacitive materials, Adv. Mater. 23 (2011) 2076–2081.
[7] H.-M. Lin, Y.-L. Chen, J. Yang, Y.-C. Liu, K.-M. Yin, J.-J. Kai, et al., Synthesis and characterization of core–shell GaP@GaN and GaN@GaP nanowires, Nano Lett. 3 (2003) 537–541.
[8] O. Hayden, A.B. Greytak, D.C. Bell, Core–shell nanowire light-emitting diodes, Adv. Mater. 17 (2005) 701–704.

[9] Q. Kuang, Z.-Y. Jiang, Z.-X. Xie, S.-C. Lin, Z.-W. Lin, S.-Y. Xie, et al., Tailoring the optical property by a three-dimensional epitaxial heterostructure: a case of ZnO/SnO_2, J. Am. Chem. Soc. 127 (2005) 11777–11784.
[10] Y.-J. Chen, G. Xiao, T.-S. Wang, F. Zhang, Y. Ma, P. Gao, et al., Synthesis and enhanced gas sensing properties of crystalline CeO_2/TiO_2 core/shell nanorods, Sens. Actuators B 156 (2011) 867–874.
[11] I.-S. Hwang, S.-J. Kim, J.-K. Choi, J. Choi, H. Ji, G.-T. Kim, et al., Synthesis and gas sensing characteristics of highly crystalline ZnO–SnO_2 core–shell nanowires, Sens. Actuators B 148 (2010) 595–600.
[12] B. Varghese, C.H. Teo, Y. Zhu, M.V. Reddy, B.V.R. Chowdari, A.T.S. Wee, et al., Co_3O_4 nanostructures with different morphologies and their field-emission properties, Adv. Funct. Mater. 17 (2007) 1932–1939.
[13] J. Park, X. Shen, G. Wang, Solvothermal synthesis and gas-sensing performance of Co_3O_4 hollow nanospheres, Sens. Actuators B 136 (2009) 494–498.
[14] J. Liu, H. Xia, L. Lu, D. Xue, Anisotropic Co_3O_4 porous nanocapsules toward high-capacity Li-ion batteries, J. Mater. Chem. 20 (2010) 1506–1510.
[15] Y. Liang, Y. Li, H. Wang, J. Zhou, J. Wang, T. Regier, et al., Co_3O_4 nanocrystals on graphene as a synergistic catalyst for oxygen reduction reaction, Nat. Mater. 10 (2011) 780–786.
[16] A.-M. Cao, J.-S. Hu, H.-P. Liang, W.-G. Song, L.-J. Wan, X.-L. He, et al., Hierarchically structured cobalt oxide (Co_3O_4): the morphology control and its potential in sensors, J. Phys. Chem. B 110 (2006) 15858–15863.
[17] D. Bekermann, A. Gasparotto, D. Barreca, C. Maccato, E. Comini, C. Sada, et al., Co_3O_4/ZnO nanocomposites: from plasma synthesis to gas sensing applications, ACS Appl. Mater. Interfaces 4 (2012) 928–934.
[18] S.O. Hwang, C.H. Kim, Y. Myung, S.-H. Park, J. Park, J. Kim, et al., Synthesis of vertically aligned manganese-doped Fe_3O_4 nanowire arrays and their excellent room-temperature gas sensing ability, Journal of Physical Chemistry C 112 (2008) 13911–13916.
[19] Z. Ai, K. Deng, Q. Wan, L. Zhang, S. Lee, Facile microwave-assisted synthesis and magnetic and gas sensing properties of Fe_3O_4 nanoroses, Journal of Physical Chemistry C 114 (2010) 6237–6242.
[20] W.-M. Zhang, X.-L. Wu, J.-S. Hu, Y.-G. Guo, L.-J. Wan, Carbon coated Fe_3O_4 nanospindles as a superior anode material for lithium-ion batteries, Adv. Funct. Mater. 18 (2008) 3941–3946.
[21] C. Feng, W. Li, C. Li, L. Zhu, H. Zhang, Y. Zhang, et al., Highly efficient rapid ethanol sensing based on $In_{2-x}Ni_xO_3$ nanofibers, Sens. Actuators B 166–167 (2012) 83–88.
[22] W. Li, C. Li, L. Zhu, C. Feng, W. Chen, W. Guo, et al., Preparation and NO_2 sensing properties of the ni-doped In_2O_3 nanofibers, Integr. Ferroelectr. 138 (2012) 71–76.
[23] J. Xu, P. Gao, T.S. Zhao, Non-precious Co_3O_4 nano-rod electrocatalyst for oxygen reduction reaction in anion-exchange membrane fuel cells, Energy Environ. Sci. 5 (2012) 5333–5533.
[24] J. Yang, H. Liu, W.N. Martens, R.L. Frost, Synthesis and characterization of cobalt hydroxide, cobalt oxyhydroxide, and cobalt oxide nanodiscs, Journal of Physical Chemistry C 114 (2010) 111–119.
[25] A. Shavel, B. Rodríguez-González, M. Spasova, M. Farle, L.M. Liz-Marzán, Synthesis and characterization of iron/iron oxide core/shell nanocubes, Adv. Funct. Mater. 17 (2007) 3870–3876.
[26] M. Kruk, M. Jaroniec, Gas adsorption characterization of ordered organic–inorganic nanocomposite materials, Chem. Mater. 13 (2001) 3169–3183.
[27] Z. Cao, J.R. Stetter, A selective solid-state gas sensor for halogenated hydrocarbons, Sens. Actuators B 5 (1991) 109–113.
[28] H. Gong, J.Q. Hu, J.H. Wang, C.H. Ong, F.R. Zhu, Nano-crystalline Cu-doped ZnO thin film gas sensor for CO, Sens. Actuators B 115 (2006) 247–251.
[29] Z. Wen, L. Tian-mo, Gas-sensing properties of SnO_2–TiO_2-based sensor for volatile organic compound gas and its sensing mechanism, Phys. B: Condens. Mat. 405 (2010) 1345–1348.
[30] S.C. Naisbitt, K.F.E. Pratt, D.E. Williams, I.P. Parkin, A microstructural model of semiconducting gas sensor response: the effects of sintering temperature on the response of chromium titanate (CTO) to carbon monoxide, Sens. Actuators B 114 (2006) 969–977.
[31] N. Yamazoe, G. Sakai, K. Shimanoe, Oxide semiconductor gas sensors, Catalysis Surveys from Asia 7 (2003) 63–75.
[32] J.-W. Yoon, J.-K. Choi, J.-H. Lee, Design of a highly sensitive and selective C_2H_5OH sensor using p-type Co_3O_4 nanofibers, Sens. Actuators B 161 (2012) 570–577.
[33] W. Guo, T. Liu, H. Zhang, R. Sun, Y. Chen, W. Zeng, et al., Gas-sensing performance enhancement in ZnO nanostructures by hierarchical morphology, Sens. Actuators B 166–167 (2012) 492–499.
[34] H.-L. Yu, L. Li, X.-M. Gao, Y. Zhang, F. Meng, T.-S. Wang, et al., Synthesis and H_2S gas sensing properties of cage-like α-MoO_3/ZnO composite, Sens. Actuators B 171–172 (2012) 679–685.
[35] C.W. Na, H.-S. Woo, I.-D. Kim, J.-H. Lee, Selective detection of NO_2 and C_2H_5OH using a Co_3O_4-decorated ZnO nanowire network sensor, Chem. Commun. 47 (2011) 5148–5150.
[36] D. Barreca, D. Bekermann, E. Comini, A. Devi, R.A. Fischer, A. Gasparotto, et al., Plasma enhanced-CVD of undoped and fluorine-doped Co_3O_4 nanosystems for novel gas sensors, Sens. Actuators B 160 (2011) 79–86.
[37] H.-R. Kim, K.-I. Choi, K.-M. Kim, I.-D. Kim, G. Cao, J.-H. Lee, Ultra-fast responding and recovering C_2H_5OH sensors using SnO_2 hollow spheres prepared and activated by Ni templates, Chem. Commun. 46 (2010) 5061–5063.

Biographies

Fengdong Qu received the bachelor degree from the College of Electronic Science and Engineering, Jilin University, China in 2012. Now, he is engaged in the synthesis and characterization of the semiconducting functional materials and gas sensors.

Juan Liu received the bachelor degree from the College of Electronic Science and Engineering, Jilin University, China in 2012. Now, she is a graduate student and interested in functional materials and gas sensors.

Ying Wang received the bachelor degree from the College of Electronic Science and Engineering, Jilin University, China in 2013. Now, she is a graduate student and interested in functional materials and gas sensors.

Shanpeng Wen received the PhD degree in the field of Polymer Chemical and Physics, Jilin University, China in 2009. Now, he is a lecturer in College of Electronics Science and Engineering, Jilin University, and mainly devoted to the research of organic material synthesis and polymeric solar cell.

Yu Chen is a full professor in the Institute of Semiconductors, Chinese Academy of Sciences. He is mainly devoted to the research of functional nanomaterials.

Xu Li is an undergraduate in College of Electronic Science and Engineering, Jilin University, China, and interested in nanomaterials and chemical sensors.

Shengping Ruan received the PhD degree of electronic science and engineering from Jilin University in 2001. Now, he is a full professor in College of Electronics Science and Engineering, Jilin University, and mainly devoted to the research of electronic functional materials and devices.